Solution Structure of Bovine Angiogenin by ^{1}H Nuclear Magnetic Resonance Spectroscopy[†,‡]

Olivier Lequin,[§] Christine Albaret,[§] François Bontems,*[,§] Geneviève Spik,[||] and Jean-Yves Lallemand[§]

Laboratoire de RMN, Département de Chimie-Synthèse Organique, URA 1308 du CNRS, Ecole Polytechnique, 91128 Palaiseau, France, and Laboratoire de Chimie Biologique, UMR 111 du CNRS, Université des Sciences et Technologies de Lille, 59655 Villeneuve d'Ascq, France

Received January 4, 1996; Revised Manuscript Received March 28, 1996[⊗]

ABSTRACT: The three-dimensional structure of bovine angiogenin has been determined using two- and three-dimensional proton NMR spectroscopy. The solution structure is very close to that recently determined by X-ray diffraction analysis. This structure appears well defined, even if five loops and one helix exhibit greater flexibility. Analysis of the active site geometry confirms the position of the Glu-118 residue which obstructs the pyrimidine binding site. There is no experimental evidence of an unobstructed conformation of angiogenin in solution. In addition, it appears that the Glu-118 and Ser-119 residues and the cell receptor binding loop may play an important role in the differences of C-terminal fragment organization and ribonucleolytic activity observed between angiogenins and ribonuclease A.

Angiogenins are 14 kDa single-chain polypeptides that are potent inducers of blood vessel neoformation (angiogenesis) at very low concentrations in the chick chorioallantoic membrane and rabbit corneal assay (Fett et al., 1985). They were first isolated in adenocarcinoma cell-culture medium but have also been found in blood serum of several mammals (Shapiro et al., 1987; Bond et al., 1993) and in cow milk (Maes et al., 1988).

The way angiogenins act is far from being completely understood. They display numerous biological activities. Human angiogenin inhibits degranulation of polymorphonuclear leukocytes (Tschesche et al., 1994) and activates second-messenger pathways in vascular smooth muscle or endothelial cells (Bicknell & Vallee, 1989). It binds to cell surface actin (Badet et al., 1989; Hu et al., 1993), supports cell adhesion on plastic surfaces (Soncin, 1992) and significantly stimulates cell migration and formation of tube-like structures (Jimi et al., 1995). Moreover, the protein is endocytosed in proliferating endothelial cells and translocates to the nucleus, where it accumulates in the nucleoli (Moroianu & Riordan, 1994). More surprisingly, angiogenins have about 33% amino acid sequence identity with pancreatic ribonuclease A (Strydom et al., 1985), including the conservation of the major active-site residues His-12, Lys-41, and His-119. They indeed exhibit a ribonucleolytic activity and seem to share the same general catalytic properties but are several orders of magnitude less active than RNase A[1] towards conventional substrates (Shapiro et al., 1986).

Among all these properties, it has been demonstrated that angiogenesis depends, at least, on the ribonucleolytic activity and on the ability to recognize a cell receptor through a region encompassing residues 60−68 and 109 (Hallahan et al., 1991). Thus a precise analysis of the active site and loop conformations in angiogenins and their comparison with the equivalent regions in RNase A (which has no angiogenic activity) would provide a structural basis to understand angiogenic properties. In this context, we have undertaken the determination of the bovine angiogenin solution structure by proton NMR (Reisdorf et al., 1994). During the refinement of our structure, crystal structures of human (Acharya et al., 1994) and bovine angiogenins (Acharya et al., 1995) were reported. Our study shows that the properties of crystal angiogenins are conserved in solution. In particular, the position of Glu-118, which is thought to play a major role in the attenuation of ribonucleolytic activity, is confirmed. We have also compared the structures of angiogenin and RNase A in a way that we hope will contribute to a better understanding of the divergent properties of these two proteins.

EXPERIMENTAL PROCEDURES

Biological Samples. Angiogenin was isolated from cow milk and samples were prepared as previously described (Reisdorf et al., 1994). Typical samples correspond to 25 mg of protein dissolved in 400 μL of 100 mmol.L^{-1} phosphate buffer, leading to a final concentration of 4 mmol L^{-1}. The pH was adjusted to 4.5 or 5.0 using microliter amount of HCl.

NMR Spectroscopy. All spectra were recorded at 308 K on a Bruker AMX600 spectrometer equipped with a triple-resonance ^{1}H/^{13}C/^{15}N gradient probe.

NOE cross-peaks were assigned on two-dimensional NOESY spectra (Kumar et al., 1980) recorded with mixing times of 40, 80, 120, and 180 ms in H_2O and 180 ms in D_2O. Experiments were processed as described (Reisdorf et al., 1994), on a Silicon Graphics R4400 workstation, using

[†] This work was supported by the French foundation for the research against cancer ARC and by Rhône Poulenc Rorer.

[‡] The coordinates have been deposited in the Brookhaven Protein Data Bank (file name 1GIO).

[§] Laboratoire de RMN.

[||] Laboratoire de Chimie Biologique.

[⊗] Abstract published in *Advance ACS Abstracts,* June 15, 1996.

[1] Abbreviations: DQF-COSY, double quantum-filtered correlation spectroscopy; FID, free induction decay; HOHAHA, homonuclear Hartmann−Hahn spectroscopy; NMR, nuclear magnetic resonance; NOE, nuclear Overhauser enhancement; NOESY, NOE spectroscopy; RNase A, ribonuclease A.

S0006-2960(96)00022-0 CCC: $12.00

the GIFA (Delsuc, 1989) and GIFC (Rouh et al., 1993) programs.

A three-dimensional NOE-NOE experiment (Breg et al., 1990) was acquired with NOESY mixing times of 150 and 170 ms. 200×146 ($t_1 \times t_2$) free-induction decays (FID) of eight scans were recorded, each FID consisting of 1024 time-domain points (total measuring time of 90 h). Time-proportional phase incrementation (TPPI) was used for sign discrimination in the ω_1 and ω_2 dimensions. Water resonance was suppressed with a WATERGATE sequence (Sklenar et al., 1993). A linear-prediction algorithm was used to increase the length of FIDs in t_1 and t_2 to 256 data points, resulting in a $256 \times 256 \times 1024$ real matrix. Prior to Fourier transformation, data were multiplied by a shifted sine-bell apodization function in the t_1 and t_2 dimensions and by a shifted square sine-bell apodization function in the t_3 dimension. A baseline correction using a morphological algorithm (Rouh et al., 1993) was applied on the transformed matrix.

Proton−deuterium exchange of the amide protons was studied on a sample lyophilized from H_2O and redissolved in pure D_2O immediately before acquisition. The residual NH signal was recorded on NOESY and HOHAHA spectra. Amide protons were divided into three groups: (1) fast exchanging protons, completely exchanged after 18 h; (2) intermediate exchanging protons, displaying a signal after 18 h; and (3) slow exchanging protons, which could be detected after 48 h. An additional DQF-COSY spectrum was recorded 3 weeks later, showing that most of the slowly exchanging protons were still detectable. Fast exchanging protons were confirmed by recording a NOESY spectrum on a sample lyophilized in D_2O and freshly dissolved in H_2O.

NMR Restraints. (a) Interproton Distance Restraints. Sequential and backbone−backbone restraints were divided into three groups and the upper limits were set to 2.8, 3.5, or 5.0 according to the intensity. Upper limits corresponding to the other long-range effects were fixed to 5.0 Å, except a few number of very strong effects set to 4.0 Å. Only strong intraresidue constraints were taken into account since the information contained in other intraresidue constraints is rather poor. They were set to a distance of 2.8 Å. In all cases, the lower bounds were set to the sum of the van der Waals radii of two protons (1.8 Å). Upper limits for distances involving methyl protons, nonstereospecifically assigned methylene, and aromatic equivalent protons were corrected appropriately when used in DIANA. No corrections were used during the refinement stage with X-PLOR. No dihedral angle constraints were introduced in so far as coupling constants could not be reliably measured by standard homonuclear experiments.

(b) Hydrogen Bond Restraints. Backbone HN·CO hydrogen bonds were identified on the basis of intermediate and slow amide protons exchange rates. Two distance restraints were used for each bond: one between the hydrogen and the acceptor atom of 2.2 Å and one between the donor heavy atom and the acceptor atom of 3.2 Å.

Structure Calculations. Structure calculations were performed with a procedure combining minimization in the dihedral space with the DIANA program (Güntert et al., 1991) followed by simulated annealing with the X-PLOR program (Brünger, 1992). Using the REDAC strategy (Güntert & Wüthrich, 1991), structures were rapidly generated with DIANA. Their analysis allowed the resolution of ambiguities in the assignment of NOE cross-peaks and the derivation of additional interproton restraints. This procedure was iterated several times by calculating at each stage a new set of structures with an improved list of restraints. The last iteration yielded 200 structures, and the 10 with the lowest target function were selected for subsequent simulated annealing. The protocol used was derived from the one described by Gippert et al. (1990). The parallhsa.pro parameter file was used in conjunction with the energy function described by Nilges et al. (1988), which contains neither electrostatic nor hydrogen bond potential and has a simple repulsive term instead of the van der Waals function. In a first stage, the DIANA structures were submitted to 6 ps simulated annealing at 1000 K, and the experimental restraint force constants were gradually increased. Because of the poor quality of the disulfide bridge geometry in the structures, the force constants of the $S\gamma-S\gamma$ bonds, $C^\beta-S^\gamma-S^\gamma$ angles, and $C^\beta-S^\gamma-S^\gamma-C^\beta$ and $C^\alpha-C^\beta-S^\gamma-S^\gamma$ dihedral angles were set to zero at the beginning of the annealing and then slowly increased together with the NOE term. In order to allow exchange of nonstereospecifically assigned β protons positions, the force constants of all angles involving a nonchiral β carbon were set to zero during the first stage of the annealing and then gradually increased in parallel with the repulsive potential in a second stage (6 ps dynamics). The cooling step consisted of 20 ps dynamics from 1000 to 0 K. Finally, a 2 ps restrained dynamics at 0 K and a minimization were carried out using the force field derived from CHARMM22 (Brooks et al., 1983) and a standard energy function but without electrostatic or hydrogen bond terms. The integration step was 1 fs, except in the last restrained dynamics where it was set to 2 fs.

Structure Analysis. Analysis of the structures was performed using X-PLOR (Brünger, 1992), PROCHECK-NMR (Laskowski et al., 1993) and Insight II (Biosym Technologies). Geometrical deviations were estimated with respect to the mean structure, calculated from the NMR structure family after best fitting of the secondary structure elements. χ_1 angular deviations were estimated using the circular variance as described by MacArthur and Thornton (1993).

Angiogenin Model Building. Bovine angiogenin model was calculated from RNase A coordinates using Biosym Homology program package.

RESULTS AND DISCUSSION

Proton Assignment

Since bovine angiogenin was directly purified from milk, it was not possible to label it. Nevertheless, an extensive use of two- and three-dimensional proton experiments had allowed the assignment of all but four spin systems (Reisdorf et al., 1994). This assignment was further completed during the course of the structure determination (Table 1). Close inspection of most cross-peaks in the two-dimensional NOESY and three-dimensional NOESY-NOESY spectra allowed the identification of the three Cys-40, Pro-92, and Cys-93 spin systems and of additional side-chain resonances. However Ala-1 spin system remained unidentified. In addition, a tentatively assigned correlation between the H^α protons of Pro-91 and Pro-92 and the absence of correlations between the H^δ protons of Pro-91 and the H^α proton of Pro-92 are consistent with a *cis* conformation of the corresponding peptidic bond.

Table 1: Additional ^{1}H NMR Chemical Shifts of Bovine Angiogenin (pH 4.5, 308 K)[a]

	^{1}H chemical shifts (ppm)			
residue	NH	$C^{\alpha}H$	$C^{\beta}H$	others
Pro-19		4.47	1.77, 0.53	$C^{\gamma}H_2$ 1.43, 1.37; $C^{\delta}H_2$ 3.56, 3.04
Met-30	8.76	4.19	1.26, 1.01	$C^{\gamma}H_2$ 1.53
Met-31	8.32	4.37	0.84	$C^{\gamma}H2$ 2.59
Cys-40	9.36	4.33	2.17, 2.02	
Pro-92		4.71*		$C^{\gamma}H_2$ 2.74*; $C^{\delta}H_2$ 3.80*
Cys-93	9.62	4.80*	3.17, 3.02	
Phe-116	9.61	4.71	2.38, 2.24	$C^{2,6}H$ 6.83; $C^{3,5}H$ 7.26; $C^{4}H$ 7.20
Glu-118	8.55	4.47	2.35, 2.08	$C^{\gamma}H_2$ 2.78, 2.67

[a] This table completes the assignment previously determined (Reisdorf et al., 1994). Chemical shifts are referenced to the water resonance, calibrated at 4.8 ppm. Resonances marked with an asterisk are tentatively assigned.

Table 2: Structural Statistics: Deviation from Experimental Restraints and Idealized Geometry[a]

	energy		rmsd			
value	E_{noe} (kJ mol^{-1})	E_{vdw} (kJ mol^{-1})	NOE (Å)	bonds (Å)	angles (deg)	impropers (deg)
average	77.3	−2823.8	0.018	0.0058	2.06	2.10
minimum	49.0	−2950.3	0.014	0.0054	1.95	1.89
maximum	99.8	−2697.9	0.021	0.0062	2.23	2.35

[a] The average values are calculated for the set of the 10 X-PLOR structures. For each value, the minimum and maximum are specified. Square-well NOE potential (E_{noe}) was calculated with a force constant of 209 kJ mol^{-1} (50 kcal mol^{-1}). The van der Waals energy term (E_{vdw}) was calculated with the CHARMM Lennard-Jones function.

Structure Analysis

Structural Statistics. Structures were calculated using a final set of 1130 distance restraints, consisting of 60 intraresidual, 365 sequential, 209 medium range, and 496 long range effects. Among them, 80 were imposed to constrain 40 hydrogen bonds deduced from the kinetics of amide proton exchange. Interestingly, the amide protons of Ile-57 and Cys-58 at the end of the helix H3 exchange slowly. The observation of $H^{\alpha}_{i-3}-HN_i$ correlations along with the absence of $H^{\alpha}_{i-4}-HN_i$ correlations raised the possibility that these residues may belong to a 3_{10} helix (characterized by $O_{i-3}\cdot HN_i$ hydrogen bonds) rather than an α helix (characterized by $O_{i-4}\cdot HN_i$ hydrogen bonds). To test this assumption, both hydrogen bond types were allowed by using ambiguous distance restraints (Nilges, 1993).

The 10 calculated structures are consistent with both experimental data and standard covalent geometry (Table 2). They display no violations greater than 0.3 Å (mean value 0.018 Å). The number of violations between 0.1 and 0.3 Å ranges from 2 to 12, most of them concerning sequential distances in loop regions. Furthermore, the covalent geometry is correct as can be judged by the low rmsd values for bond lengths and bond angles. The van der Waals energy term is large and negative indicating that there are no bad nonbonded contacts. Most of the backbone torsion angles for non-glycine residues (94%) fall in the generally allowed regions of the Ramachandran plot, with the exception of some residues in loop regions and at the ends of the molecule (Figure 1). In particular, the ϕ angles of the three residues Arg-35, Asp-60, and Asn-110 are almost always positive. For two residues, Arg-35 and Asn-110, this is supported by the observation of strong intraresidual $HN-H^{\alpha}$ NOE correlations. In the case of Asp-60, the sequential and the intraresidual correlations are superimposed, preventing the evaluation of the intraresidual NOE intensity.

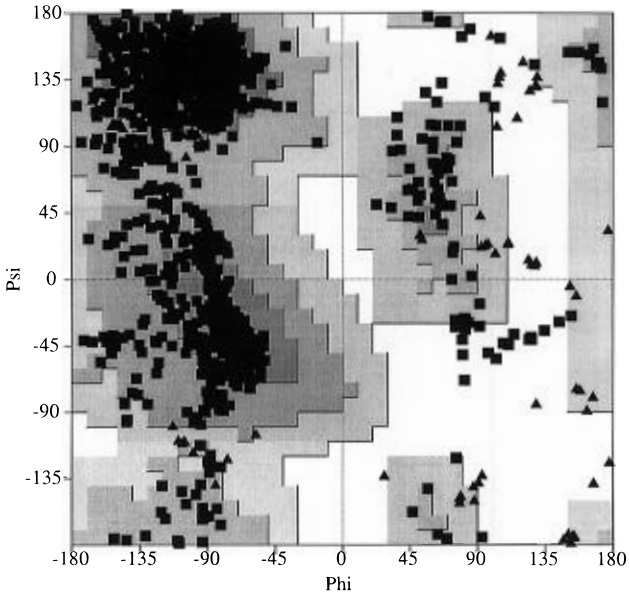

FIGURE 1: Ramachandran (ϕ,ψ) plot for the 10 structures of bovine angiogenin. The different regions of the Ramachandran plot are represented by levels of shading (from dark gray to white: most favorable, allowed, generously allowed, and disallowed). Glycine residues are represented by triangles. This plot was generated with the PROCHECK-NMR program (Laskowsky et al., 1993).

Description of the Structure. A superposition of the backbones of the 10 refined structures is shown in Figure 2. In general, the conformation is well defined, with the exception of the two unconstrained termini (residues 1−4 and 122−125). The average root mean square deviation calculated from the mean structure for backbone atoms is 1.49 Å but decreases to 0.77 Å if the N and C termini are omitted (residues 5−121).

As emphasized by the MOLSCRIPT diagram (Figure 2), the three-dimensional structure is kidney-shaped with approximate dimensions 40 Å × 45 Å × 28 Å and consists of the three helical regions and seven β strands previously identified (Reisdorf et al., 1994). The core of the molecule comprises two antiparallel β sheets of three (S1) and four strands (S2). The two structures are not in fact independent and their two central β strands can be best described as part of a unique antiparallel twisted β sheet, giving the bilobate appearance. The N-terminal H1 helix is approximately parallel to strand B7 of sheet S2, while H2 and H3 helices are disposed on one side of sheets S1 and S2, respectively, with their axis approximately perpendicular to the strand direction. An extensive hydrophobic core lies at the junction of helix H1, helix H3, and sheets S1 and S2, connecting the two lobes. The N-terminal H1 helix makes contacts with both lobes, preferentially with strands B1 and B7, through residues Tyr-7, Phe-10, and His-14. Helix H3 is connected to the C-terminal part of strand B6 by a disulfide bridge (58−108) and makes several hydrophobic contacts through residues Ile-54 and Ile-57 to the core of the structure. Helix H2 is packed against the triple stranded sheet S1, through residues Tyr-26 and Met-30 and is tethered to strand B4 by a disulfide bridge (27−82). In addition, a third disulfide bond (40−93) attaches the loop between strands B4 and B5 (residues 86−94) to the irregular region 36−42.

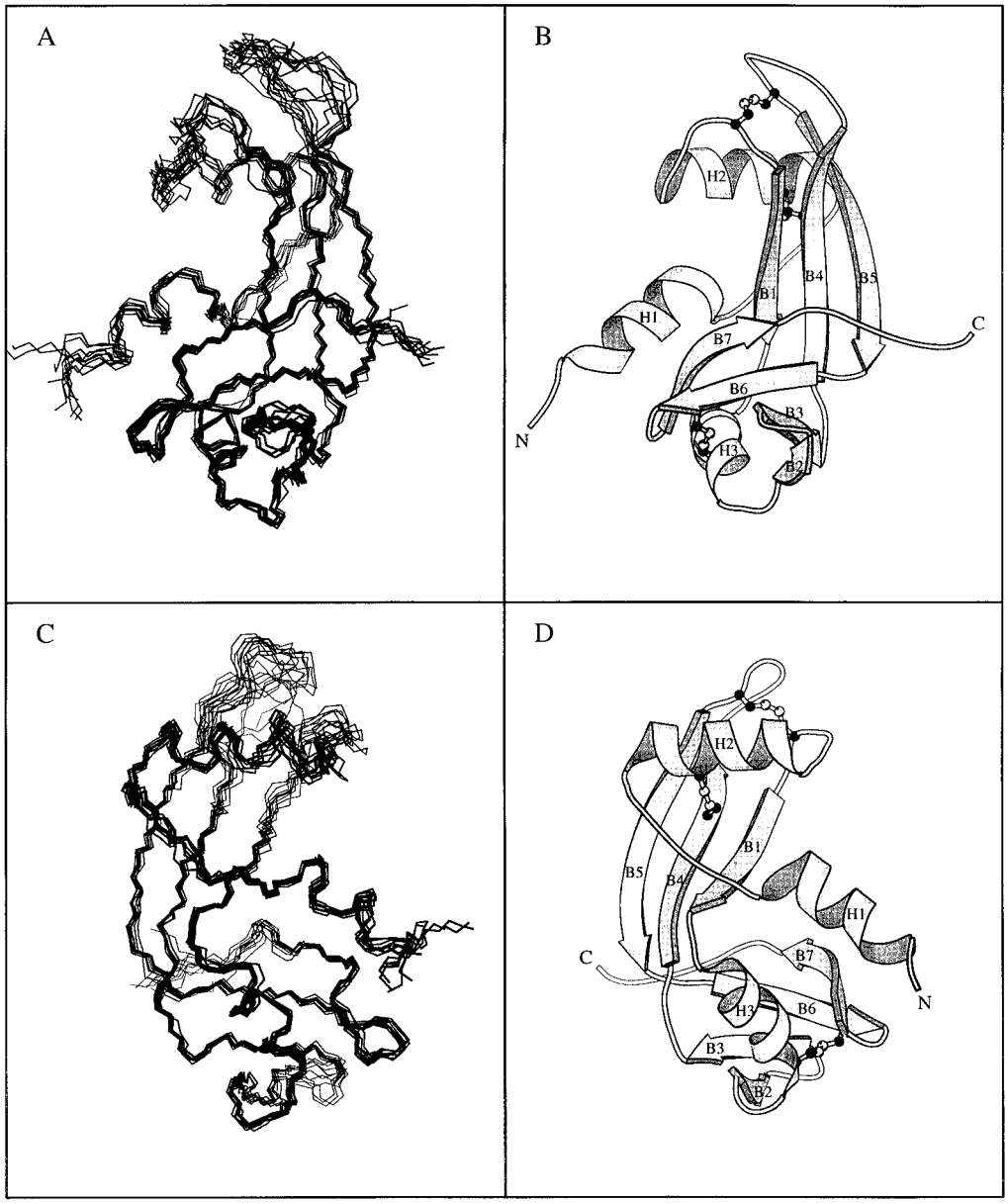

FIGURE 2: Three-dimensional solution structure of bovine angiogenin. (Panels A and C) Backbone superposition of the 10 structures, viewed from two different angles. Residues 1−4 and 122−125, which are disordered, have been omitted. The 10 structures were fitted to the mean structure. (Panels B and D) MOLSCRIPT diagram (Kraulis, 1991) of the polypeptide fold of the mean structure. The secondary structure elements are labeled according to their occurrence in the sequence.

As mentioned above, a direct analysis of NOESY data raised the possibility that H3 C-terminal end could be a 3_{10} helix rather than an α-helix. This hypothesis was confirmed by the fact that, in all the structures, Ile-57 and Cys-58 amide protons are involved in hydrogen bonds with Ile-54 and Lys-55 carboxylic oxygens, respectively. In contrast, all H1 residues exhibit $H^{\alpha}_{i-4}-HN_i$ NOE cross-peaks, in addition to the $H^{\alpha}_{i-3}-HN_i$ NOE cross-peaks, indicating that this helix is completely in an α conformation. In the case of H2, things are less clear. Due to the lower number of NOE cross-peaks in this region, the helix is poorly defined, providing no way to distinguish between both types.

Dynamics of the Structure. The mean deviation from the average structure, calculated on backbone atoms, is plotted in Figure 3. It is shown that the rmsd of most residues lies under 0.5 Å. However, five segments present a larger dispersion: the two unconstrained extremities, the 86−94 long loop connecting strands B4 and B5 (1.77 Å), the 67−69 RGD loop (1.01 Å), and the 35−42 segment following helix H2 (1.08 Å). On the opposite, most secondary structural elements are well defined (0.46 Å), although it can be noted that H2 helix, in particular in its C-terminal region, and H1 to a lesser extent, present a greater deviation than H3.

As generally observed in solvent exposed regions, the increased disorder of all loops is not surprising and is likely to reflect greater flexibility. Similarly, the larger dispersion of H1 and H2, when compared to H3, may also be due to an increase in the local flexibility or unstability. In support of this hypothesis, it is noteworthy that most protons of the β sheets and of helix H3 remain unexchanged after several days at room temperature, whereas all H1 and H2 protons are exchanged after 24 h (Figure 3).

Comparison with Crystal Structures of Angiogenins. During the refinement of our structure, the X-ray determination of both human and bovine angiogenin at 2.4 and 1.5 Å resolution, respectively, has been reported (Acharya et al., 1994, 1995). Since the atomic coordinates of bovine angiogenin are not yet available from the Brookhaven Protein

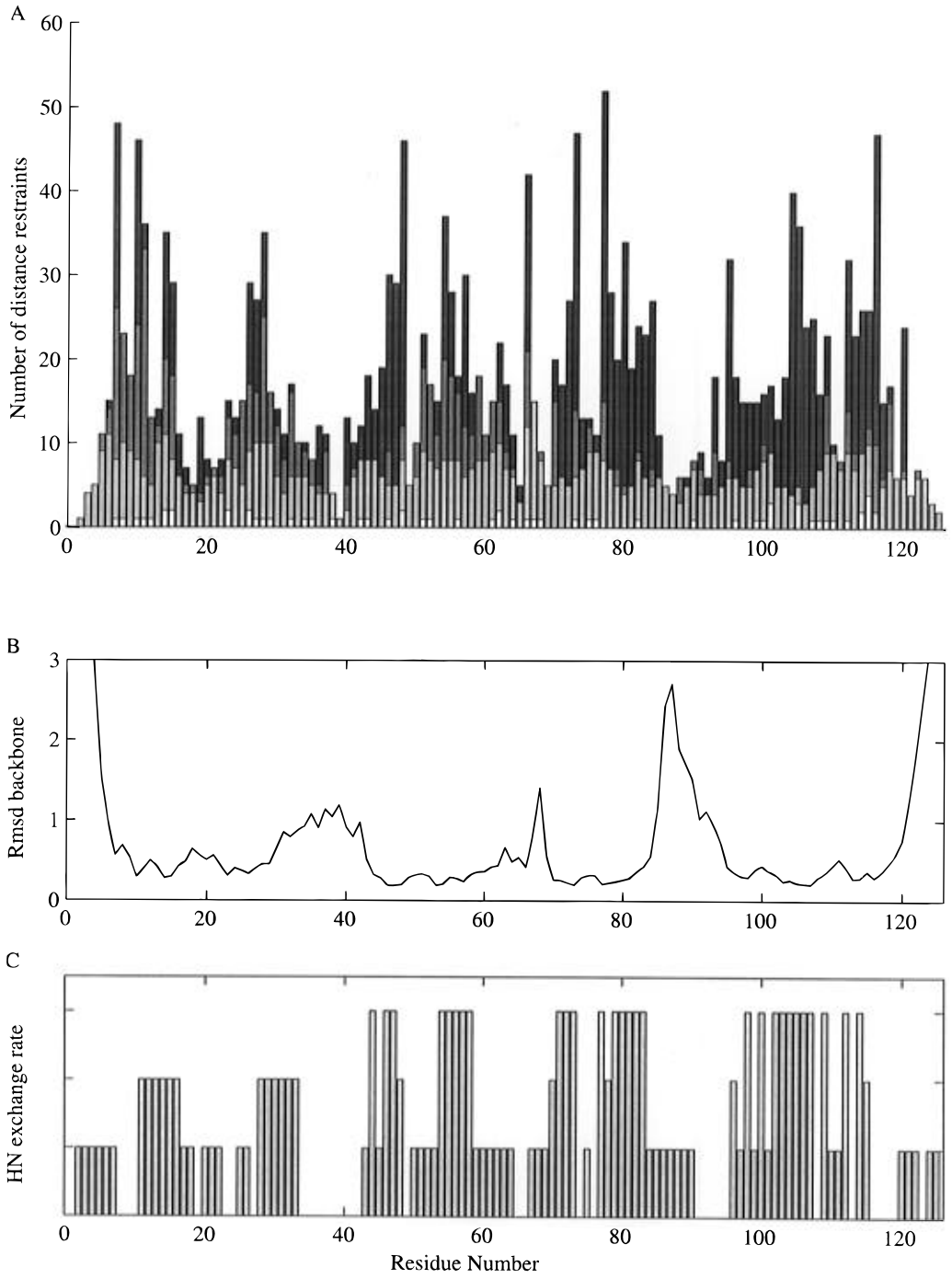

FIGURE 3: Representation of distance restraints, mean deviation of backbone atoms, and amide proton exchange rates as a function of the protein sequence. (A) Distribution of NOEs along the sequence. Intraresidue NOEs are shown in white, sequential NOEs in light gray, medium-range NOEs (*i*, *i*+2 to *i*+4) in dark gray, and long-range NOEs in black. (B) Rmsd of backbone atoms from their position in the mean structure. (C) Rates of NH/ND exchange. Fast, medium, and slow exchanging protons are represented by small, intermediate, and tall bars, respectively. The absence of bar corresponds either to prolines or to protons not identified in the exchange experiments.

Data Bank, no detailed comparison of the two models could be made. However, they seem to be very similar in terms of global shape, backbone overall fold, and definition of secondary structure elements. Human angiogenin sequence is 66% identical to that of bovine and differs by two single-residue deletions at both termini (Maes et al., 1988). The rms difference of residue 6−118 backbone atom positions is 1.43 Å (1.01 Å for secondary structure elements). The main difference resides in the C-terminal region (Figure 4). In human angiogenin, residues 117−121 form a 3_{10} helix, whereas the corresponding segment in bovine angiogenin differs after residue Ser-119 in orientation and positioning of hydrophobic side chains. Beyond Phe-120, which side chain is engaged in a hydrophobic cluster with Val-105, the region seems rather flexible.

Receptor Binding Site

Angiogenin function requires at least an intact ribonucleolytic activity and the ability to recognize a cell receptor (Hallahan et al., 1991). Mutagenesis studies showed that the putative receptor binding site in human angiogenin comprised the residues Arg-66, Glu-67, and Asn-68. In bovine angiogenin, the corresponding residues are Arg-67, Gly-68, and Asp-69, forming an RGD sequence. As RGD sequences often constitute recognition sites by membrane receptor proteins of the integrin family, it has been proposed

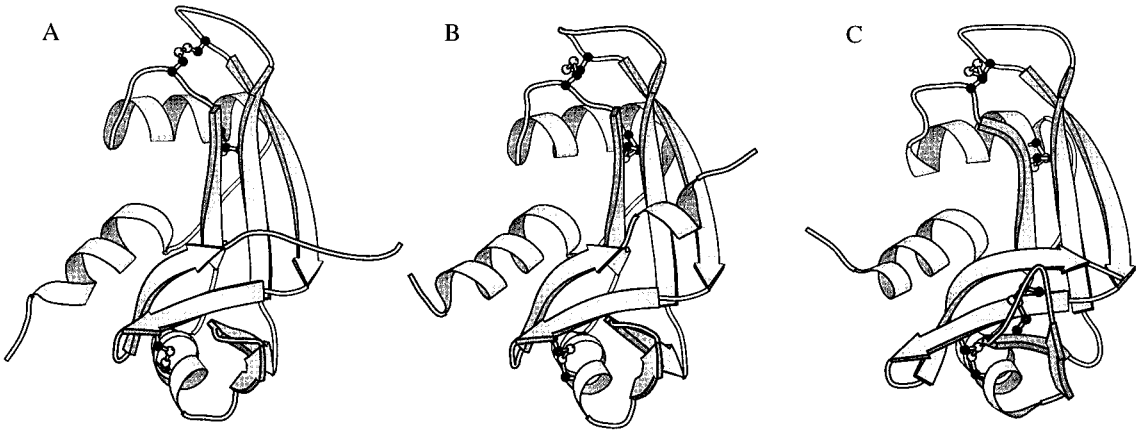

FIGURE 4: Comparison of the polypeptide folds of angiogenins and RNase A. The MOLSCRIPT diagram of the backbone of bovine angiogenin mean structure (A), human angiogenin (B), and RNase A (C) crystal structures are represented. Structures of human angiogenin (Acharya et al., 1994) and RNase A (Wlodawer et al., 1988) were downloaded from the Brookhaven Protein Data Bank (entry codes 1ANG and 7RSA, respectively).

Table 3: Comparison of the Conformation of the $R_{67}G_{68}D_{69}$ Residues in the 10 Bovine Angiogenin Structures with RGD Proteins[a]

rmsd	1FNA	1FOD	4GCR	1TEN	1DEC	ANG1	ANG2	ANG3	ANG4	ANG5	ANG6	ANG7	ANG8	ANG9	ANG10
1FNA		1.28	1.21	1.41	1.22	1.19	1.21	1.58	1.33	1.04	1.55	1.09	1.35	1.58	1.20
1FOD			0.30	1.23	0.78	1.02	1.06	1.67	1.34	0.93	1.62	0.83	1.29	1.60	1.02
4GCR				1.30	0.93	1.15	1.19	1.69	1.43	1.05	1.65	0.96	1.36	1.63	1.14
1TEN					0.71	1.09	1.14	0.70	0.75	0.70	0.66	0.79	0.60	0.60	1.10
1DEC						0.67	0.72	1.23	0.78	0.35	1.17	0.32	0.77	1.13	0.66

[a] The rms deviations are calculated for N, C, C^{α}, and C^{β} atoms. The 10 NMR structures of bovine angiogenin are indicated by ANG1 to ANG10. The other abbreviations used are the PDB entry codes: 1FNA, tenth type-III module of fibronectin (Dickinson et al., 1994); 1FOD, foot and mouth disease virus VP1 protein (Logan et al., 1993); 4GCR, γB-crystallin (Najmudin et al., 1993); 1TEN, third fibronectin type-III repeat of tenascin (Leahy et al., 1992); 1DEC, decorsin (Krezel et al., 1994). 1FNA, 1FOD, 4GCR, and 1TEN are crystal structures. In the solution structure of decorsin, the RGD region is well defined (Krezel et al., 1994); therefore, one NMR structure has been chosen to calculate the rmsds.

that human and bovine angiogenins may recognize cells in different ways (Maes et al., 1988). To date, however, this suggestion is not supported by biological evidence.

Analysis of angiogenin X-ray structure shows that the geometry of its RGD sequence differs substantially from the foot-and-mouth disease virus (FMDV) VP1 protein and γB-crystallin, which are known to bind integrins (Acharya et al., 1995). This led the authors to the suggestion that this sequence does not constitute a true RGD motif. However, a conformational change of this peptide upon binding to cell surface remains all the more possible as the RGD loops are known to be flexible and as the Arg-67 and Asp-69 residues are directly involved in crystal lattice contacts (Acharya et al., 1995).

In solution, the RGD sequence of angiogenin shares properties with those of many integrin binding proteins. It forms a short solvent-exposed loop at the apex of the B2−B3 sheet and seems flexible, as suggested by the greater rmsd, the reduced number of NOEs, and the fast amide proton exchange (Figure 3), though this mobility would need further investigation by means of relaxation measurements.

We have compared the RGD loop conformations of our 10 structures with those of several known integrin binding proteins (Table 3). As observed for the crystal structure, the rmsd calculated on backbone and Cβ atoms is rather high when compared with the VP1 protein and the γB-crystallin. However, these values are of the same order as those observed between the γB-crystallin or the VP1 protein on the one hand and tenascin or decorsin on the other hand. Moreover, both the latter are quite close to some of our angiogenin conformers. The observed variability among the integrin binding proteins suggests either an inherent flexibility or the existence of distinct active RGD conformations conferring specificity in recognition by different integrins. In this context, some of our structures may have an appropriate conformation to integrin recognition. Thus, the differences underlined with γB-crystallin and VP1 protein might not provide sufficient grounds to exclude that the angiogenin RGD sequence may participate in the common RGD-type interaction.

Similarity with RNase A

Angiogenins are the only angiogenic factors endowed with a ribonuclease activity. They indeed belong to the pancreatic ribonuclease superfamily, as shown by 33% sequence identity and structural similarity with RNase A.

As also shown by crystal structures comparison (Acharya et al., 1995), the global folds of ribonuclease A and bovine angiogenin are closely related (Figure 4). The rms deviation, calculated on the alignment of 106 equivalent α-carbon atoms, is 1.60 Å. In particular secondary structure elements are very similar in both proteins (rmsd 1.26 Å) and the main hydrophobic cores are conserved. A major difference involves the "RGD loop" between strands B2 and B3 which is longer in RNase A and stabilized by a fourth disulfide bridge. This structural difference correlates with a divergence in biological function (see below).

The dynamic behavior of RNase A, observed by NMR (Santoro et al., 1993), is also related to that of bovine angiogenin. Variability is quite similar in loop regions. Furthermore, helix H2 appears looser than helix H3, as noted for angiogenin.

Ribonucleolytic Active Site. The ribonucleolytic active site is a long cleft at the junction of helix H1, strand B1, and strand B7, running approximately parallel to strand B7. Three

Table 4: Structural Statistics for Active Site Residues: Number of Experimental Distance Constraints and Conformational Variability

residue	NOEs	side chain NOEs[a]	rmsd (Å)[b]	χ_1 circular variance
His-14	35	18 (13)	0.32	0.002
Lys-41	10	3	1.51	0.614
Thr-45	19	7	0.43	0.136
His-115	26	9 (5)	0.48	0.005
Phe-116	47	39 (33)	0.71	0.001
Glu-118	17	6	1.03	0.234

[a] Number of medium- and long-range NOEs involving side chain protons; values given in parentheses are for aromatic protons. [b] The rmsd is calculated for heavy atoms.

major sites have been delineated in RNase A: a P1 site, at which phosphodiester bond cleavage occurs, a B1 site for pyrimidine binding, and a B2 site for purine binding (Eftink & Biltonen, 1987). The homology between angiogenins and RNase A includes the conservation of most residues of these sites.

Positions of His-14, Lys-41, His-115, and Thr-45, which are the major residues of P1 and B1 sites, are generally well-defined (Table 4) and, as already mentioned for the crystal structure, quite similar to those in RNase A (Figure 5). Interestingly, NMR spectroscopy enables one to determine unambiguously the orientation of histidine side chains, through the observation of Hϵ1 and Hδ2 protons. We show that the imidazole rings of His-14 and His-115 in bovine angiogenin have the same orientations as in RNase A (determined by neutron diffraction and NMR), which is a further indication of conserved catalytic properties.

The imidazole ring of His-14 is slightly tilted with respect to its position in RNase A and the crystal structure of angiogenin. However, this angle variation may be too small to be significant. The side chain of Lys-41 shows a higher dispersion, related to the small number of observed NOEs (Table 4). This is to be compared with the *B* factors in the RNase A crystal which are significantly higher than those of the other active site residues (Wlodawer et al., 1988). His-115 side chain shows a larger variation than His-14 (Table 4) but displays a unique conformation. Interestingly, an alternative position of the side chain of the RNase A equivalent residue His-119 has been reported in the solution (Rico et al., 1991; Santoro et al., 1993) and in some crystal structures (Borkakoti et al., 1982). In fact there is a dynamic equilibrium in solution between two positions for the His-119 side chain, dependent on pH conditions and phosphate concentration (Rico et al., 1991). The observation of this alternative position would require the identification of NOEs between His-115 and methyl protons of Val-114 (residue equivalent to Val-118 in RNase A). These NOEs could not be identified owing to the strong overlap in the corresponding region of the NOESY spectra. Therefore, an alternative conformation of His-115 in bovine angiogenin can not be excluded. At last, 33 NOE correlations were observed between Phe-116 aromatic protons and seven other residues (in particular Phe-10, His-14, Thr-45, and Glu-118), which results in a significant rotation (about 50°) of the aromatic ring with respect to the corresponding Phe-120 residue in RNase A. This rotation could be relevant in so far as Phe-120 in RNase A has been proposed to be involved in pyrimidine stacking (Zegers et al., 1994).

Molecular Basis for Enzymatic Differences between RNase A and Angiogenin

Although their ribonucleolytic activity is crucial for angiogenesis, angiogenins are extremely weak ribonucleases toward conventional RNase A substrates and differ in specificity. Their efficiency toward poly(U) or poly(C) is several orders of magnitude below those of RNase A while they seem to be specific for 28S and 18S rRNA *in vitro* (Shapiro et al., 1986) or for tRNA when injected in *Xenopus* oocytes (Saxena et al., 1992). Analysis of both human and bovine angiogenin crystal structures has revealed that the side chain of Glu-118 (Gln-117 in human angiogenin) obstructs the pyrimidine binding site (Acharya et al., 1994, 1995). This, together with mutagenesis data (Russo et al., 1994), provides a convincing structural basis to account for the very low ribonucleolytic activity.

Solution Conformation of Glu-118 Side Chain and Orientation of the C Terminus Region. In solution, NOE correlations involving the side chain γ protons of Glu-118 are observed with the imidazole ring Hϵ1 proton of His-14 and the aromatic protons of Phe-116, providing unambiguous positioning of Glu-118 side chain in the active site (Figure 5). This residue is not as well-defined as the major active site residues (Table 4) and two main conformations, which differ by the orientation of the γ-carboxylic group, may be distinguished in the structures. In one subpopulation, the position is quite similar to that reported for crystal structures, in which the carboxylate group hydrogen bonds to HN and HO$^{\gamma}$ of Thr-45. Alternatively, the carboxylate group is oriented in the opposite direction, preventing the formation of both hydrogen bonds, but the side chain position remains altogether unfavorable for pyrimidine binding. This local variability could reflect a lack of experimental constraints. However, it should be mentioned that none of the two Thr-45 amide and hydroxylic protons appear protected. The amide proton exchanges rapidly, and the hydroxylic proton was not observed in any spectrum.

The obstruction of the pyrimidine binding site in the uncomplexed state suggests that a conformational change would be necessary to allow ligand binding (Acharya et al., 1994; Russo et al., 1994). This is not likely to be achieved by a simple modification of the Gln-117 (human) or Glu-118 (bovine) side-chain orientation alone. The mutation of Gln-117 to Gly or Ala causes only a slight increase in activity, which remains much weaker than that of RNase A (Russo et al., 1994). In fact, the structure of the C-terminal fragment is different in RNase A and in angiogenins, indicating that a reorganization of this whole region could be necessary (Acharya et al., 1994; Russo et al., 1994). Comparison of this region in RNase A and angiogenins shows the following: the three backbones are identical up to Asp-117 (with the numbering of bovine angiogenin), where RNase A diverges, while the two angiogenins remain similar up to Ser-119. This suggests that the difference in C-terminus organization could reside primarily in residues Glu-118 and Ser-119.

The existence of a unique set of chemical shifts excludes the possibility of a slow equilibrium between two similarly populated conformations. On the other hand no NOE suggesting a second conformation of the C-terminal part of the molecule was found. Thus, the hypothesis of two populated forms in fast equilibrium seems also unlikely. Therefore, it can be assessed that only one conformation of

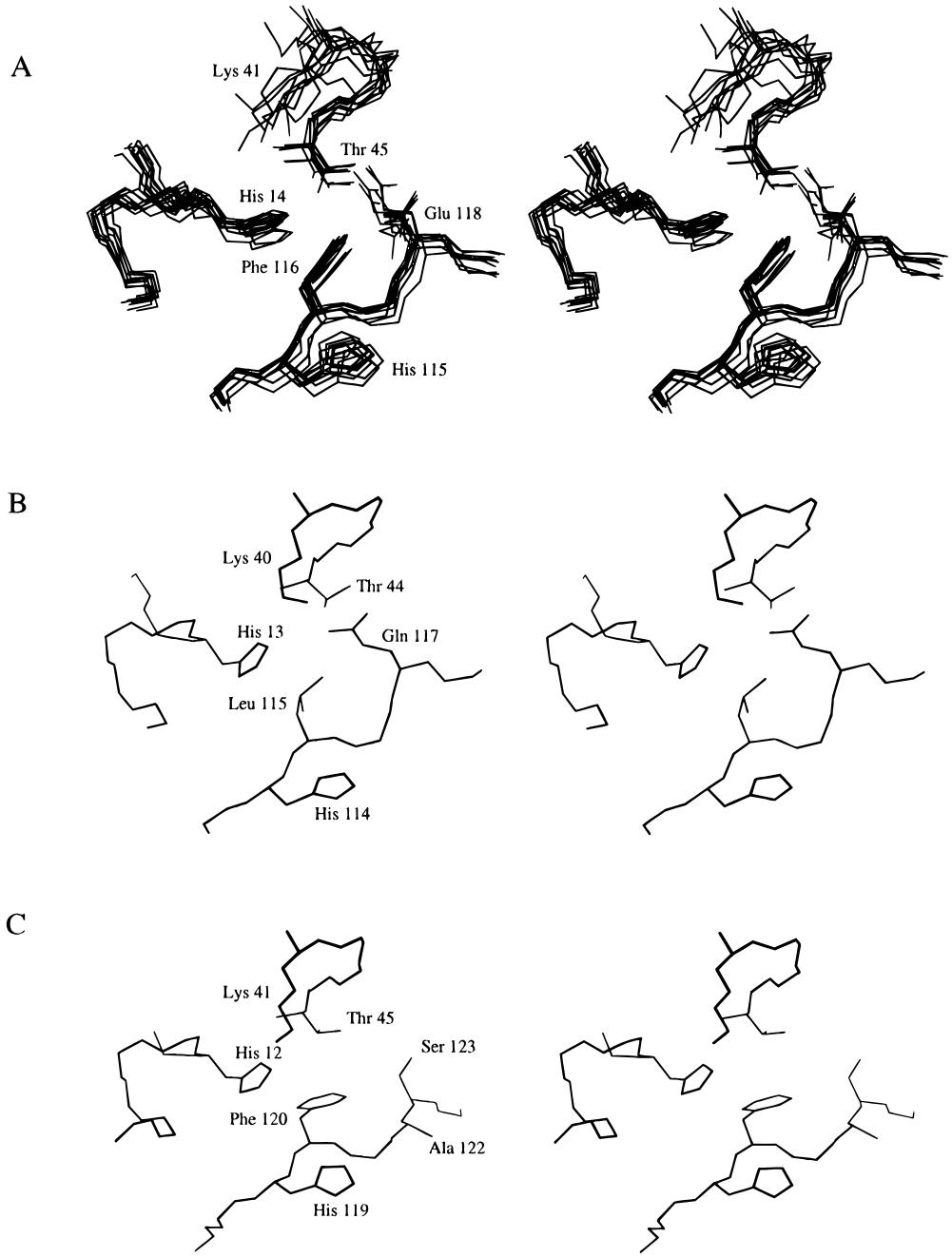

FIGURE 5: Stereoview of the active sites of angiogenins and RNase A. (A) Superimposition of the 10 bovine angiogenin NMR structures. The His-14, Lys-41, and His-115 catalytic residues together with the Thr-45 and Phe-116 B1 residues are labeled. Note the position of Glu-118, which lies in the B1 site. (B) View of the human angiogenin active site. Phe-116 and Glu-118 are conservatively replaced by Leu-115 and Gln-117. (C) View of the RNase A active site. Note the different orientations of Phe-120 aromatic ring and of the Ala-122 side chains. This latter is pointing in the opposite direction to that of Glu-118.

angiogenin exists in solution. A putative conformer with an unobstructed B1 site would be either very minor or would occur during, rather than prior to, ligand binding. Since the structures of human and bovine angiogenin have been resolved in quite the same conditions in both NMR and crystallographic studies (pH range: 4.5−5.2), it would be of interest to study whether another conformer could be observed in different conditions.

To investigate the molecular basis of the different C-terminal orientations, we built a model of angiogenin in which the C-terminal part consisted in an extended fragment as in RNase A (Figure 6). In this model, the side chains of Glu-118 and Ser-119 are oriented in opposite directions with respect to their positions in angiogenin. Glu-118 side chain points toward a hydrophobic core, which would destabilize the structure and may explain the presence, in all ribonucleases, of an alanine at this position. A relevant exception is the turtle pancreatic ribonuclease, which has an arginine residue and is strikingly similar to angiogenins (Beintema et al., 1988). In addition, the position of Ser-119, as observed in angiogenins, would not be favorable in the RNase A context, due to the location of the Lys-66 side chain which belongs to the divergent B2−B3 loop (see next paragraph).

Divergence of the B2−B3 Loop. As already mentioned, an essential difference between angiogenins and RNase A lies in the organization of the B2−B3 loop. In RNase A, this loop is seven residues long and comprises Asn-67, Gln-69, and Asn-71, proposed to be involved, together with residue Glu-111, in purine interactions (Fontecilla-Camps et al., 1994). In contrast, the loop is reduced to three residues

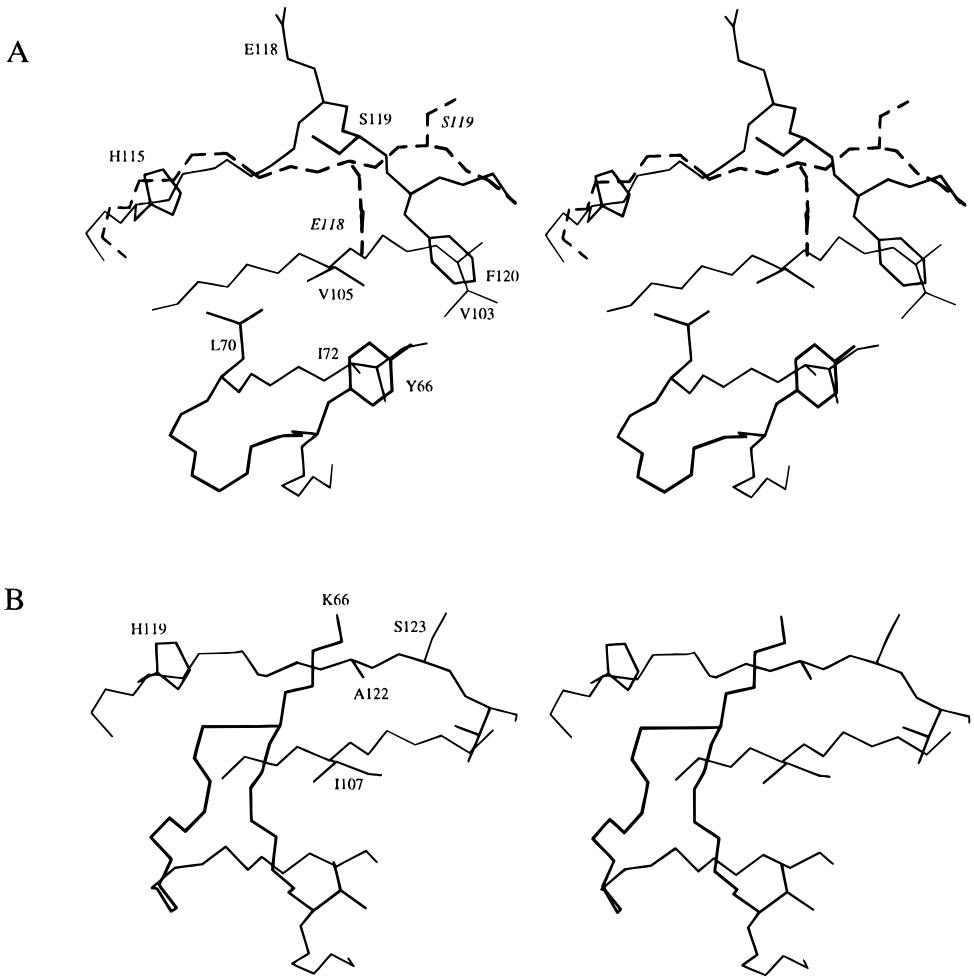

FIGURE 6: Comparison of the C-terminal region and B2−B3 loop of bovine angiogenin and RNase A. (A) Stereoview of the C-terminal region and the B2−B3 loop of the best bovine angiogenin structure. The corresponding C-terminal segment (dashed line, italic labelling), as build by homology with RNase A, has been superimposed, showing that Glu-118 would point toward a hydrophobic core defined by residues Val-103, Val-105 and Phe-120. (B) Stereoview of the corresponding region in RNase A. Note the orientation of Lys-66 (deleted in angiogenins) which occupies the region delineated by Ser-119 side chain in bovine angiogenin structure. As evidenced by the figure, the Ala-122 and Ser-123 side chains have orientations opposite to those of Glu-118 and Ser-119.

in angiogenins and forms the putative cell receptor binding site. The only conserved residue, Asn-69 cannot be appropriately superimposed with any of those aforementioned. However, angiogenin Glu-109 residue (homologous to RNase A Glu-111) has a similar position and could thus also be involved in purine binding. Nevertheless, it is worth noting that these two residues have only a limited role both in RNase A (Tarragona-Fiol et al., 1993) and in angiogenin (Curran et al., 1993).

Another difference between the two loops is the deletion of RNase A Lys-66. In addition to its possible role in the divergences of the C-terminal regions, the absence of this residue implies a modification of the charge distribution at the surface of angiogenin, in particular in the vicinity of the active site, which could influence substrate binding and therefore may be related with the differences of specificity.

CONCLUSION

Two major differences distinguish angiogenins from the other members of the pancreatic ribonuclease superfamily: the presence of an angiogenic activity and the modification of the enzymatic properties. The relationship between ribonucleolytic activity and angiogenic activity, though necessary, remains so far unclear. In order to understand the divergence between RNase A and angiogenins, numerous structure/function relationship studies have been undertaken, and there are now three structures of angiogenins available.

From a structural point of view, the divergence between angiogenins and RNase A resides mainly in the C-terminal region and the loop connecting strands B2 and B3. This loop in RNase A encompasses several residues involved in downstream or peripheral substrate binding (Lys-66, Asn-67, Gln-69, Asn-71). In angiogenins these residues are not conserved, and furthermore this region constitutes a cell receptor binding motif. At last, this loop could influence the conformation of the C terminus as Lys-66 in RNase A is close to the position of Ser-119 in bovine angiogenin.

Since angiogenins are endowed with a ribonucleolytic activity, it remains to be investigated how a conformational change in the obstructed pyrimidine binding site could occur and how a ribonucleotide molecule may be recognized as a substrate. Our solution structure provides a background for further interaction studies by NMR spectroscopy.

ACKNOWLEDGMENT

Bovine angiogenin was purified by J.-P. Decottignies, in the laboratory of biological chemistry (UMR 111 du CNRS, Université des Sciences et Technologies de Lille) headed by Prof. A. Verbert. Calculations were performed using the resources of the French center for supercomputing applica-

tions IDRIS. We gratefully acknowledge A. Benaskeur for expert technical assistance and Dr. D. Abergel for fruitful discussion. We also thank Dr. F. Dardel and Dr. A. Siriwardena for their comments.

REFERENCES

Acharya, K. R., Shapiro, R., Allen, S. C., Riordan, J. F., & Vallee, B. L. (1994) Crystal structure of human angiogenin reveals the structural basis for its functional divergence from ribonuclease, *Proc. Natl. Acad. Sci. U.S.A. 91*, 2915−2919.

Acharya, K. R., Shapiro, R., Riordan, J. F., & Vallee, B. L. (1995) Crystal structure of bovine angiogenin at 1.5-Å resolution, *Proc. Natl. Acad. Sci. U.S.A. 92*, 2949−2953.

Badet, J., Soncin, F., Guitton, J.-D., Lamare, O., Cartwright, T., & Barritault, D. (1989) Specific binding of angiogenin to calf pulmonary artery endothelial cells, *Proc. Natl. Acad. Sci. U.S.A. 86*, 8427−8431.

Beintema, J. J., Schüller, C., Irie, M., & Carsana, A. (1988) Molecular evolution of the ribonuclease superfamily, *Prog. Biophys. Mol. Biol. 51*, 165−192.

Bicknell, R., & Vallee, B. L. (1989) Angiogenin stimulates endothelial cell prostacyclin secretion by activation of phospholipase A2, *Proc. Natl. Acad. Sci. U.S.A. 86*, 1573−1577.

Bond, M. D., Strydom, D. J., & Vallee, B. L. (1993) Characterization and sequencing of rabbit, pig and mouse angiogenins: discernment of functionally important residues and regions, *Biochim. Biophys. Acta 1162*, 177−186.

Borkakoti, N., Moss, D. S., & Palmer, R. A. (1982) Ribonuclease A: least-squares refinement of structure at 1.45 Å resolution, *Acta Crystallogr. Sect. B 38*, 2210−2217.

Breg, J. N., Boelens, R., Vuister, G. W., & Kaptein, R. (1990) 3D NOE-NOE spectroscopy of proteins. Observation of sequential 3D NOE cross peaks in Arc repressor, *J. Magn. Reson. 87*, 646−651.

Brooks, B. R., Bruccoleri, R. E., Olafson, B. D., States, D. J., Swaminathan, S., & Karplus, M. (1983) CHARMM: a program for macromolecular energy, minimization, and dynamics calculations, *J. Comput. Chem. 4*, 187−217.

Brünger, A. T. (1992) *X-PLOR version 3.1, A system for X-ray crystallography and NMR*, Yale University Press, New Haven and London.

Curran, T. P., Shapiro, R., & Riordan, J. F. (1993) Alteration of the enzymatic specificity of human angiogenin by site-directed mutagenesis, *Biochemistry 32*, 2307−2313.

delCardayré, S. B., & Raines, R. T. (1995) A residue to residue hydrogen bond mediates the nucleotide specificity of ribonuclease A, *J. Mol. Biol. 252*, 328−336.

Delsuc, M.-A. (1989) A new maximum entropy processing algorithm, with applications to nuclear magnetic resonance experiments, in *Maximum Entropy and Bayesian Methods* (Skilling, J., Ed.) pp 285−290, Kluwer Academic Publishers, Dordrecht, The Netherlands.

Dickinson, C. D., Veerapandian, B., Dai, X. P., Hamlin, R. C., Xuong, N., Ruoslahti, E., & Ely, K. (1994) Crystal structure of the tenth type III cell adhesion module of human fibronectin, *J. Mol. Biol. 236*, 1079−1092.

Eftink, M. R., & Biltonen, R. L. (1987) in *Hydrolytic Enzymes* (Neuberger, A., & Brocklehurst, K., Eds.) pp 333−376, Elsevier Science Publishers B. V., Amsterdam.

Fett, J. W., Strydom, D. J., Lobb, R. R., Alderman, E. M., Bethune, J. L., Riordan, J. F., & Vallee, B. L. (1985) Isolation and characterization of angiogenin, an angiogenic protein from human carcinoma cells, *Biochemistry 24*, 5480−5486.

Fontecilla-Camps, J. C., de Llorens, R., le Du, M. H., & Cuchillo, C. M. (1994) Crystal structure of ribonuclease A·d(ApTpApApG) complex, *J. Biol. Chem. 269*, 21526−21531.

Gippert, G. P., Yip, P. F., Wright, P. E., & Case, D. A. (1990) Computational methods for determining protein structures from NMR data, *Biochem. Pharmacol. 40*, 15−22.

Güntert, P., & Wüthrich, K. (1991) Improved efficiency of protein structure calculations from NMR data using the program DIANA with redundant dihedral angle constraints, *J. Biomol. NMR 1*, 447−456.

Güntert, P., Braun, W., & Wüthrich, K. (1991) Efficient computation of three-dimensional protein structures in solution from nuclear magnetic resonance data using the program DIANA and the supporting programs CALIBA, HABAS and GLOMSA, *J. Mol. Biol. 217*, 517−530.

Hallahan, T. W., Shapiro, R., & Vallee, B. L. (1991) Dual site model for the organogenic activity of angiogenin, *Proc. Natl. Acad. Sci. U.S.A. 88*, 2222−2226.

Hu, G.-F., Strydom, D. J., Fett, J. W., Riordan, J. F., & Vallee, B. L. (1993) Actin is a binding protein for angiogenin, *Proc. Natl. Acad. Sci. U.S.A. 90*, 1217−1221.

Jimi, S., Ito, K., Kohno, K., Ono, M., Kuwano, M., Itagaki, Y., & Ishikawa, H. (1995) Modulation by bovine angiogenin of tubular morphogenesis and expression of plasminogen activator in bovine endothelial cells, *Biochem. Biophys. Res. Commun. 211*, 476−483.

Kraulis, P. J. (1991) MOLSCRIPT: a program to produce both detailed and schematic plots of protein structures, *J. Appl. Crystallogr. 24*, 946−950.

Krezel, A. M., Wagner, G., Seymour-Ulmer, J., & Lazarus, R. A. (1994) Structure of the RGD protein decorsin: conserved motif and distinct function in leech proteins that affect blood clotting, *Science 264*, 1944−1947.

Kumar, A., Ernst, R. R., & Wüthrich, K. (1980) A two-dimensional nuclear Overhauser enhancement (2D NOE) experiment for the elucidation of complete proton-proton cross-relaxation networks in biological macromolecules, *Biochem. Biophys. Res. Commun. 95*, 1−6.

Laskowski, R. A., MacArthur, M. W., Moss, D. S., & Thornton, J. M. (1993) PROCHECK: a program to check the stereochemical quality of protein structures, *J. Appl. Crystallogr. 26*, 283−291.

Leahy, D. J., Hendrickson, W. A., Aukhil, I., & Erickson, H. P. (1992) Structure of a fibronectin type III domain from tenascin phased by MAD analysis of the selenomethionyl protein, *Science 258*, 987−991.

Logan, D., Abu-Ghazaleh, R., Blakemore, W., Curry, S., Jackson, T., King, A., Lea, S., Lewis, R., Newman, J., Parry, N., Rowlands, D., Stuart, D., & Fry, E. (1993) Structure of a major immunogenic site on foot-and-mouth disease virus, *Nature 362*, 566−568.

MacArthur, M. W., & Thornton, J. M. (1993) Conformational analysis of protein structures derived from NMR data, *Proteins 17*, 232−251.

Maes, P., Damart, D., Rommens, C., Montreuil, J., Spik, G., & Tartar, A. (1988) The complete amino acid sequence of bovine milk angiogenin, *FEBS Lett. 241*, 41−45.

Moroianu, J., & Riordan, J. F. (1994) Nuclear translocation of angiogenin in proliferating endothelial cells is essential to its angiogenic activity, *Proc. Natl. Acad. Sci. U.S.A. 91*, 1677−1681.

Najmudin, S., Nalini, V., Driessen, H. P. C., Slingsby, C., Blundell, T. L., Moss, D. S., & Lindley, P. F. (1993) Structure of bovine γ-B (γ-II) crystallin at 1.47 Å resolution, *Acta Crystallogr. Sect. D 49*, 223.

Nilges, M. (1993) A calculation strategy for the structure determination of symmetric dimers by ^{1}H NMR, *Proteins 17*, 297−309.

Nilges, M., Clore, G. M., & Gronenborn, A. M. (1988) Determination of three-dimensional structures of proteins from interproton distance data by hybrid distance geometry-dynamical simulated annealing calculations, *FEBS Lett. 229*, 317−324.

Reisdorf, C., Abergel, D., Bontems, F. Lallemand, J.-Y., Decottignies, J. P., & Spik, G. (1994) Proton resonance assignments and secondary structure of bovine angiogenin, *Eur. J. Biochem. 224*, 811−822.

Rico, M., Santoro, J., Gonzalez, C., Bruix, M., Neira, J. L., Nieto, J. L., & Herranz, J. (1991) 3D structure of bovine pancreatic ribonuclease A in aqueous solution: an approach to tertiary structure determination from a small basis of ^{1}H NMR NOE correlations, *J. Biomol. NMR 1*, 283−298.

Rouh, A., Delsuc, M.-A., Bertran, G., & Lallemand, J.-Y. (1993) The use of classification in baseline correction of FT NMR spectra, *J. Magn. Reson. 102*, 357−359.

Russo, N., Shapiro, R., Acharya, K. R., Riordan, J. F., & Vallee, B. L. (1994) Role of glutamine-117 in the ribonucleolytic activity of human angiogenin, *Proc. Natl. Acad. Sci. U.S.A. 91*, 2920−2924.

Santoro, J., Gonzalez, C., Bruix, M., Neira, J. L., Nieto, J. L., Herranz, J., & Rico, M. (1993) High-resolution three-dimensional structure of ribonuclease A in solution by nuclear magnetic resonance spectroscopy, *J. Mol. Biol. 229*, 722−734.

Saxena, S. K., Rybak, S. M., Davey, R. T., Youle, R. J., & Ackerman, E. J. (1992) Angiogenin is a cytotoxic, tRNA-specific ribonuclease in the RNase A superfamily, *J. Biol. Chem. 267*, 21982−21986.

Shapiro, R., Riordan, J. F., & Vallee, B. L. (1986) Characteristic ribonucleolytic activity of human angiogenin, *Biochemistry 25*, 3527−3532.

Shapiro, R., Strydom, D. J., Olson, K. A., & Vallee, B. L. (1987) Isolation of angiogenin from normal human plasma, *Biochemistry 26*, 5141−5146.

Sklenar, V., Piotto, M., Leppik, R., & Saudek, V. (1993) Gradient-tailored water suppression for ^{1}H-^{15}N HSQC experiments optimized to retain full sensitivity, *J. Magn. Reson. 102*, 241−245.

Soncin, F. (1992) Angiogenin supports endothelial and fibroblast cell adhesion, *Proc. Natl. Acad. Sci. U.S.A. 89*, 2232−2236.

Strydom, D. J., Fett, J. W., Lobb, R. R., Alderman, E. M., Bethune, J. L., Riordan, J.F., & Vallee, B. L. (1985) Amino acid sequence of human tumor derived angiogenin, *Biochemistry 24*, 5486−5494.

Tarragona-Fiol, A., Eggelte, H. J., Harbron, S., Sanchez, E., Taylorson, C. J., Ward, J. M., & Rabin, B. R. (1993) Identification by site-directed mutagenesis of amino acids in the B2 subsite of bovine pancreatic ribonuclease A, *Protein Eng. 6*, 901−906.

Tschesche, H., Kopp, C., Hörl, W. H., & Hempelmann, U. (1994) Inhibition of degranulation of polymorphonuclear leukocytes by angiogenin and its tryptic fragment, *J. Biol. Chem. 269*, 30274−30280.

Wlodawer, A., Svensson, L. A., Sjölin, L., & Gilliland, G. L. (1988) Structure of phosphate-free ribonuclease A refined at 1.26 Å, *Biochemistry 27*, 2705−2717.

Zegers, I., Maes, D., Dao-Thi, M.-H., Poortmans, F., Palmer, R., & Wyns, L. (1994) The structures of RNase A complexed with 3′-CMP and d(CpA): active site conformation and conserved water molecules, *Protein Sci. 3*, 2322−2339.

BI960022R